BIOENGINEERING

Injectable hydrogel microspheres with self-renewable hydration layers alleviate osteoarthritis

Yiting Lei[1]†, Yuping Wang[1]†, Jieliang Shen[1], Zhengwei Cai[2], Chen Zhao[1], Hong Chen[1], Xiaoji Luo[1], Ning Hu[1]*, Wenguo Cui[2]*, Wei Huang[1]*

Introducing hydration layers to hydrogel microspheres (HMs) by coating the surface with liposomes can effectively reduce friction. However, the lubrication can be inactivated when the surface coatings are damaged. To endow HMs with the ability to form self-renewable hydration layers and maintain cellular homeostasis, rapamycin-liposome–incorporating hyaluronic acid–based HMs (RAPA@Lipo@HMs) were created using microfluidic technology and photopolymerization processes. The RAPA@Lipo@HMs improve joint lubrication by using a smooth rolling mechanism and continuously exposing liposomes on the outer surface to form self-renewable hydration layers via frictional wear. In addition, the released autophagy activator (rapamycin)–loaded cationic liposomes can target negatively charged cartilage through electrostatic interactions and maintain cellular homeostasis by increasing autophagy. Furthermore, the in vivo data showed that the RAPA@Lipo@HMs can alleviate joint wear and delay the progression of osteoarthritis. The RAPA@Lipo@HMs can provide efficient lubrication and potentially alleviate friction-related diseases such as osteoarthritis.

INTRODUCTION

Efficient biolubrication at biological contacting surfaces (e.g., synovial joints or the oral cavity) is essential to ensure function (*1*). However, lubrication impaired by mechanical or biological factors can lead to severe implications such as osteoarthritis or xerostomia (*2*, *3*). Therefore, improving biolubrication while maintaining cellular homeostasis can effectively treat friction-related diseases (*4*). Hydrogel microspheres (HMs) are micrometer-sized spherical hydrogels comprising three-dimensionally cross-linked hydrophilic polymers (*5*, *6*). With excellent injectability and biocompatibility, HMs can act similar to ball bearings to reduce friction at sliding interfaces via a rolling mechanism, making them attractive candidates for biolubricants (*5*, *7*–*10*). The surface lubrication properties of rolling elements can notably affect their rolling performances (*8*, *11*, *12*). Hydration layers formed by the interaction of water molecules with charged ions or zwitterions can substantially reduce friction (*13*). Therefore, adding hydration layers to HMs can achieve a synergistic effect of hydration lubrication and ball-bearing lubrication, expanding the application prospects of HMs in the field of biolubrication.

HMs coated by polymer brushes or liposomes can have hydration layers on their outer surfaces and can provide efficient lubrication (*13*–*15*). Liu *et al.* (*16*) found that poly(3-sulfopropyl methacrylate potassium salt) brush–coated poly(*N*-isopropyl acrylamide) HMs provided a low coefficient of friction (COF) by hydration lubrication. In our previous work, gelatin methacrylate HMs modified with a poly sulfobetaine methacrylate brush showed better lubrication performance than unmodified HMs (*8*). Zheng *et al.* (*11*) reported that coating silk microspheres with a phospholipid liposomal layer could achieve adequate hydration lubrication and improve the rolling of microspheres. However, the coated layers could be torn during the friction process because of their poor wear resistance, and the hydration layers broke down when the coated layers disappeared (*17*–*20*). As a result, the lubrication performance of HMs can decrease if the hydration layers fail to be renewed or replenished (*21*). Therefore, it is a critical challenge to renew the damaged hydration layers on HMs.

Lipids on the cartilage surface can complex with hyaluronic acid (HA) and form robust hydration layers to reduce the COF (*22*). In addition, the hydration layers can be renewed in the presence of lipids in the synovial fluid (SF) once the surface-attached lipid layers are broken (*23*, *24*). Sorkin *et al.* (*23*) were inspired by these characteristics, and they evaluated the lubrication behavior of the liposomal layer in a liposome dispersion (a liposome reservoir), determining that liposomal layers can provide reversible and reproducible lubrication, and the hydration layers can be renewed in a liposome reservoir. However, liposomes in the external reservoir may have poor access to the intersurface region (*25*). Alternatively, developing a liposome reservoir as a biolubricant whose hydration layers can self-renew during friction has broader application prospects. Therefore, a liposome reservoir incorporating liposomes within HA-based HMs that can form self-renewable hydration layers on the outer surfaces and create a stable lubrication effect at biological interfaces, especially at joint interfaces where sustained friction occurs, is needed.

In this study, rapamycin (RAPA)–loaded hydrogenated soy phosphatidylcholine (HSPC) liposomes were integrated into a methacrylated HA (HAMA) matrix through noncovalent interactions, forming injectable cationic liposome–incorporating HMs with self-renewing hydration lubrication and cellular homeostasis maintenance using microfluidic technology and photopolymerization processes (Fig. 1A). As shown in Fig. 1B, the hybrid HMs can improve joint lubrication via a rolling mechanism. The hybrid HMs can serve as liposome reservoirs to continuously expose liposomes on the outer surfaces to form self-renewable hydration layers as HMs wear under friction, increasing rotational mobility and promoting smooth

[1]Department of Orthopedics, The First Affiliated Hospital of Chongqing Medical University, Orthopedic Laboratory of Chongqing Medical University, No. 1 Youyi Road, Yuzhong District, Chongqing 400016, P. R. China. [2]Department of Orthopaedics, Shanghai Key Laboratory for Prevention and Treatment of Bone and Joint Diseases, Shanghai Institute of Traumatology and Orthopaedics, Ruijin Hospital, Shanghai Jiao Tong University School of Medicine, 197 Ruijin 2nd Road, Shanghai 200025, P. R. China.
*Corresponding author. Email: huncqjoint@yeah.net (N.H.); wgcui80@hotmail.com (W.C.); huangw511@163.com (W.H.)
†These authors contributed equally to this work.

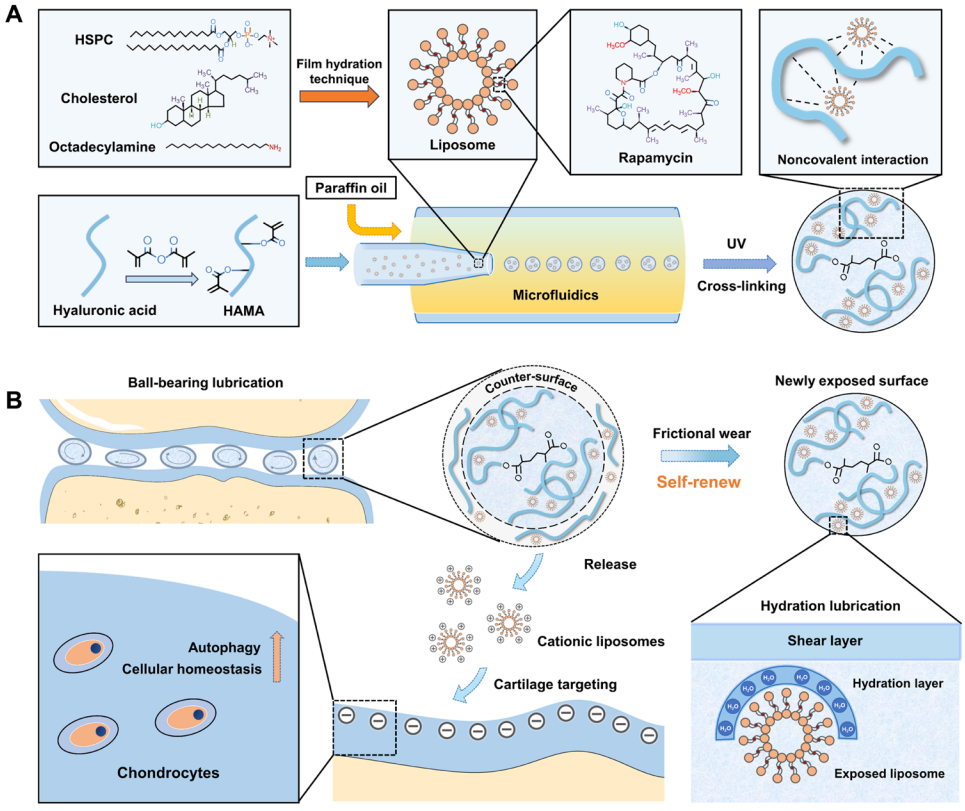

Fig. 1. The principle and fabrication of RAPA@Lipo@HMs. (**A**) The fabrication of RAPA@Lipos, photocrosslinkable HAMA matrix, and microfluidic RAPA@Lipo@HMs. (**B**) The design of RAPA@Lipo@HMs for treating osteoarthritis based on combining hydration lubrication and ball-bearing lubrication and maintaining cellular homeostasis.

rolling. Furthermore, the autophagy activator (RAPA)–loaded cationic liposomes released from HMs can target negatively charged cartilage through electrostatic interactions and maintain cellular homeostasis by increasing autophagy. The constructed liposome-incorporating hybrid HMs have great therapeutic potential in treating friction-related diseases such as osteoarthritis (*26*, *27*).

RESULTS

Fabrication and characterization

HA was chosen as the building block of the HMs. As an extracellular matrix component, HA has excellent biocompatibility (*28*). In addition, HA molecules can complex with liposomes to form a liposome reservoir via noncovalent interactions and expose the intensely hydrated phosphocholine groups of liposomes to form hydration layers (*22*, *29*). HA was modified with methacrylic anhydride to endow HA with photocurability. Proton nuclear magnetic resonance (^{1}H NMR) spectra confirmed the successful grafting of methacrylate groups. The degree of methacrylation of HAMA was 52.91% (fig. S1).

In this study, HSPC lipids were used to prepare liposomes because of their robust nature, which enables the liposomes to provide efficient boundary lubrication at physiologically high pressures (*26*). The transmission electron microscopy (TEM) micrograph of liposomes prepared using a thin-film hydration method revealed a spherical multilamellar vesicle morphology (Fig. 2A). As shown in Fig. 2B, the liposomes had a positive zeta potential of 45.4 ± 5.6 mV, which would facilitate liposome targeting of negatively charged glycosaminoglycan chains inside the cartilage (*30*). In this study, 1,1′-dioctadecyl-3,3,3′,3′-tetramethylindocarbocyanine (Dil)–labeled liposomes were used to supervise the liposome attachment to the cartilage surface. As shown in fig. S2, red fluorescence was distributed in the cartilage surface, confirming the liposome's cartilage-targeting property. However, the cartilage matrix is largely composed of dense type II collagen (Col2), and nanoparticles larger than 200 nm would be stuck to the cartilage surface, creating a barrier to chondrocyte-targeted therapy (*31*). As shown in Fig. 2C, the average size of the liposomes was 102.3 ± 35.2 nm with a polydispersity index (PDI) of 0.132, displaying good dispersity. Furthermore, the small size of the liposomes (smaller than 200 nm) is beneficial for penetrating cartilage. Because RAPA needs to access the interior of cells to unfold their activity, intracellular transport is critical for RAPA delivery (*32*). Cationic liposomes can interact with negatively charged cells and are readily internalized by them (*33*). In this study, red fluorescence signals were observed within the chondrocytes after incubating with Dil-labeled cationic liposomes (fig. S3), indicating that the cationic liposomes were taken up by the chondrocytes.

In this study, the Lipo@HMs were formed through photopolymerization of liposome-HAMA pre-gel droplets (fig. S4) generated from a microfluidic device (fig. S5). Light microscopy images showed that the microfluidic Lipo@HMs were well dispersed with intact morphological features (Fig. 2D), and the particle sizes were 208.36 ± 7.37 μm with a narrow size distribution (Fig. 2E), which may facilitate the rolling of HMs and help in the ball-bearing lubrication (*8*). HMs containing DiI–labeled liposomes were examined by laser scanning

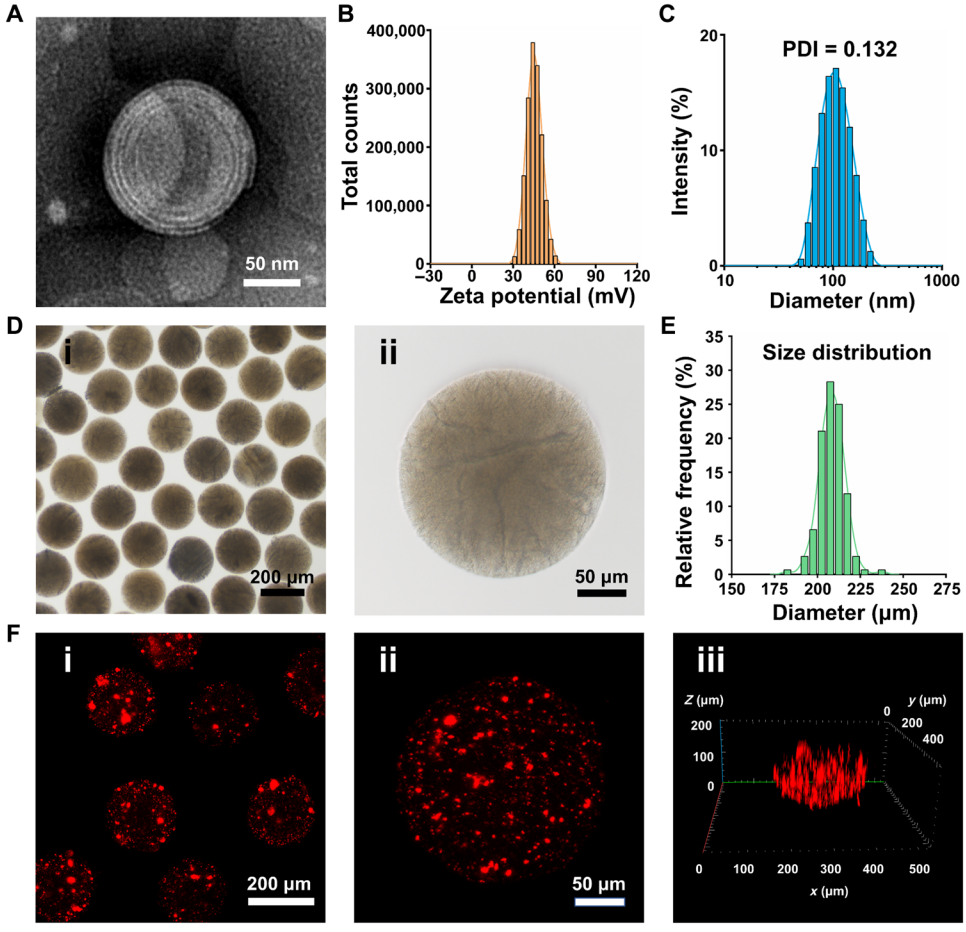

Fig. 2. Characterization of liposomes and Lipo@HMs. (**A**) TEM image of the liposome. (**B**) Zeta potential distribution of liposomes. (**C**) Size distribution of liposomes. (**D**) Bright-field images of Lipo@HMs: (i) dispersed Lipo@HMs and (ii) mono-Lipo@HM. (**E**) Size distribution of Lipo@HMs. (**F**) LSCM images of Lipo@HMs: (i) dispersed Lipo@HMs, (ii) mono-Lipo@HM, and (iii) the z-stack fluorescent images of Lipo@HM.

confocal microscopy (LSCM) to confirm the successful incorporation of liposomes. As shown in Fig. 2F, red fluorescence was distributed within the HMs, indicating that liposomes were successfully integrated into the HMs.

Self-renewing lubrication performance

To characterize the entire lubrication process of the newly prepared Lipo@HMs, the Lipo@HMs were subjected to a 3600-s friction test on a universal materials tester (UMT-3) (Fig. 3A). As shown in Fig. 3B, there are four stages in the entire lubrication course. Stage one (gray area; 0 to 300 s) is where the COF exhibited a slow downward trend, indicating that most of the outer layers of the Lipo@HMs, which contained few liposomes, were wearing off, and the Lipo@HMs were exposing liposomes on the outer surfaces to form self-renewable hydration layers according to frictional wear. Stage two (blue area; 300 to 1200 s) is where the COF was stabilized at approximately 0.03, indicating that Lipo@HMs had exposed a sufficiently large number of liposomes, and water molecules surrounding the Lipo@HMs were attached strongly to the phosphocholine headgroups of exposed liposomes to form self-renewable hydration layers, thus exerting a stable lubrication effect. Stage three (purple area; 1200 to 2700 s) is where the COF showed a slow upward trend, indicating that the Lipo@HMs were squeezed out of the confined region. Stage four (green area; 2700 to 3600 s) is where the COF showed a rapid upward trend, indicating a shift from wet to dry friction because of water loss. However, unlike the constant sliding motion, the gait cycle has a stance phase and a swing phase (*34*). During the swing phase, there is a brief separation between the upper and lower articular surface, which would allow both Lipo@HMs and water back into the frictional areas. Therefore, the lubrication process of the Lipo@HMs in the joint is mainly the first two stages.

To verify the ability to form self-renewable hydration layers, the surface morphologies of the Lipo@HMs before (newly prepared Lipo@HMs) and after friction (worn Lipo@HMs) were compared using scanning electron microscopy (SEM). As seen from Fig. 3C, only one liposome was observed on the outer surface of the newly prepared Lipo@HM in a random SEM field. It might happen because most liposomes were encapsulated inside the HMs. In addition, without the protection from the hydrogel network, the liposomes remaining on the outer surfaces could be damaged and removed during the oil-removing process. Unlike the newly prepared Lipo@HMs, many liposomes were exposed on the outer surfaces of the worn Lipo@HMs (Fig. 3D), indicating that the Lipo@HMs can expose

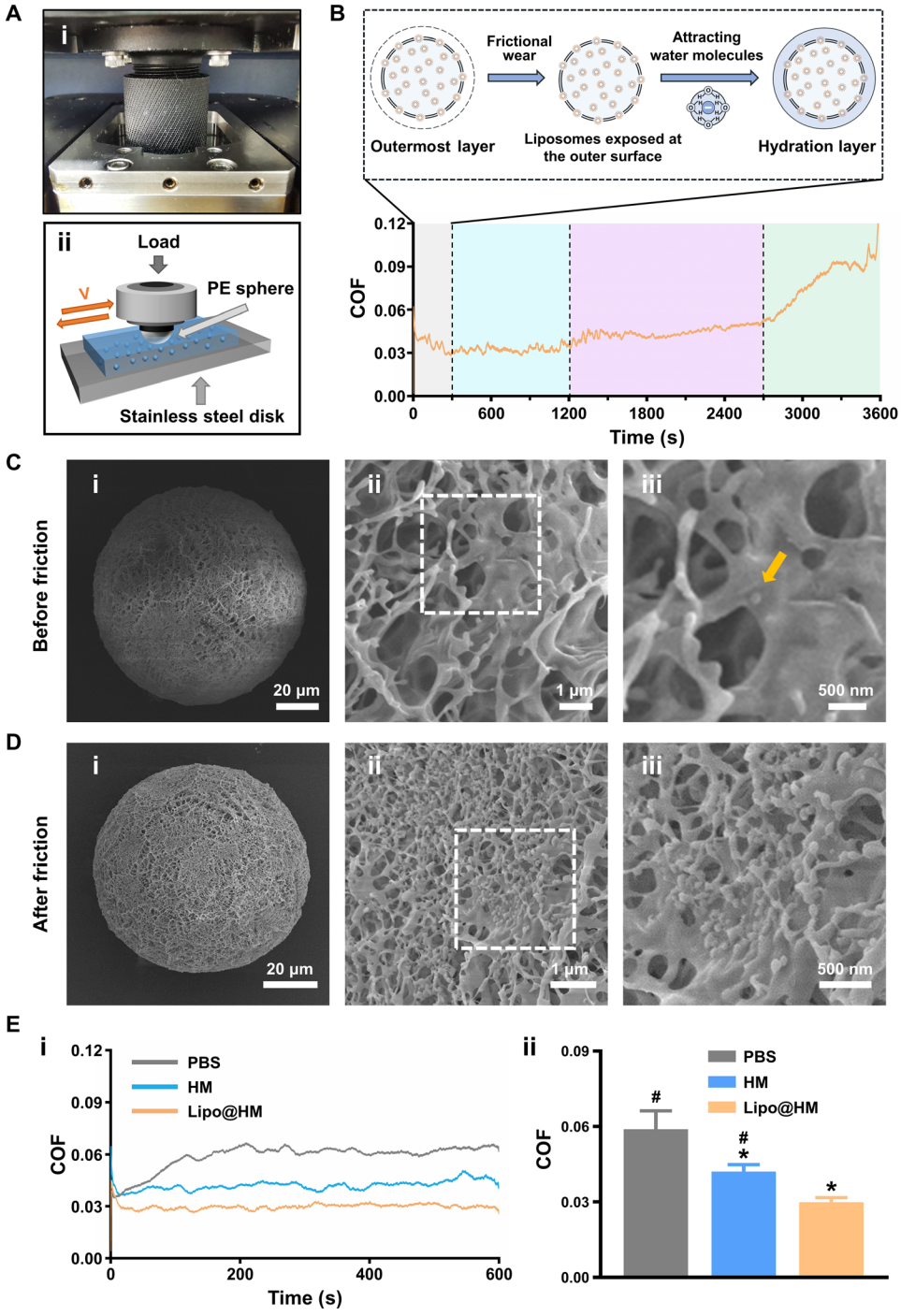

Fig. 3. Lubrication performances of Lipo@HMs. (**A**) (i) Photograph and (ii) schematic of the UMT-3. PE, polyethylene. (**B**) COF-time curve for the newly prepared Lipo@HMs. (**C**) SEM images of newly prepared Lipo@HM from (i) the overall view and (ii and iii) the local view. The yellow arrow in the image indicates the location of liposome. (**D**) SEM images of the worn Lipo@HM from (i) the overall view and (ii and iii) the local view. (**E**) (i) COF-time curves and (ii) COF histograms for PBS, HMs, and the worn Lipo@HMs (# and * indicate $P < 0.05$ in comparison with the Lipo@HM and PBS groups, respectively). Photo credit: Yiting Lei, The First Affiliated Hospital of Chongqing Medical University.

liposomes on the outer surfaces to form self-renewable hydration layers as HMs wear under friction.

We then evaluated the lubrication performances of phosphate-buffered saline (PBS), liposome-free HMs, and the worn Lipo@HMs under the same test conditions. As shown in Fig. 3E, compared with PBS (COF: 0.06), HMs decreased the COF to 0.04 via the rolling mechanism. Unlike the above friction test results, the worn Lipo@HMs with sufficient liposomes exposed on the outer surfaces directly decreased the COF to 0.03 without a slowly decreasing process. Furthermore, the wear track in the worn Lipo@HM group was

narrower and shallower than in the PBS and HM groups (fig. S6). These results suggest that the Lipo@HMs can serve as liposome reservoirs to expose liposomes on the outer surfaces to form self-renewable hydration layers in response to frictional wear, providing efficient lubrication during friction.

Furthermore, the biolubricating effects of the worn Lipo@HMs were characterized in the presence of model SF under physiological joint pressure. As shown in fig. S7, after replacing PBS with SF, the COF values of the HMs (0.04) and Lipo@HMs (0.03) remained unchanged because lipids in the SF had poor access to the intersurface region, thus the limited effect on the COF values (*25*). Lipo@HMs had better lubricating effects than the HMs and model SF under joint-simulating conditions, providing more evidence for joint-lubricating potential.

Degradation property

Slower biodegradation rates of a lubricating biomaterial can prolong the in vivo retention time, which may aid sustained lubrication (*8*, *9*). As shown in Fig. 4A, the HMs showed a relatively rapid degradation trend in the presence of hyaluronidase and were completely degraded on day 42. The Lipo@HMs also showed a similar degradation trend to HMs through day 7, followed by a relatively slow degradation trend, and were completely degraded on day 63. The different degradation trend between the HMs and Lipo@HMs might be because the Lipo@HMs can expose liposomes on the outer surfaces during degradation, and the hydration layers formed surrounding the Lipo@HMs can act as a physical barrier against hyaluronidase and thus retard the degradation process (Fig. 4B) (*8*, *9*).

Drug loading and release properties

RAPA has poor bioavailability, a narrow therapeutic index, and is rapidly cleared from the body as a water-insoluble drug (*35*, *36*). Liposome encapsulation can enhance the aqueous solubility of RAPA and provide slow and sustained release of RAPA (*37*, *38*). In addition, incorporating liposomes within HMs can further increase the stability of the drug delivery system, which may contribute to local drug delivery (*39*). As shown in Fig. 4C, the encapsulation efficiency of RAPA in liposomes and Lipo@HMs was 87.55 ± 6.49% and 67.39 ± 4.06%, respectively. This decrease in encapsulation efficiency may be because of drug leakage and the removal of exposed liposomes during the oil-removing process (*39*). In the subsequent drug release experiment, the cumulative release profiles of RAPA loaded in liposomes and Lipo@HMs were biphasic, with an initial rapid release period (3 days) followed by a slower release phase. In addition, the Lipo@HMs (28 days) showed a prolonged drug release compared with the liposomes (14 days) (Fig. 4D), indicating that the Lipo@HMs can serve as an efficient drug delivery system for controlled drug release.

Biocompatibility test

As a biolubricant, the RAPA-liposome–incorporating HMs (RAPA@Lipo@HMs) should have good biocompatibility (*8*, *40*). Thus, a

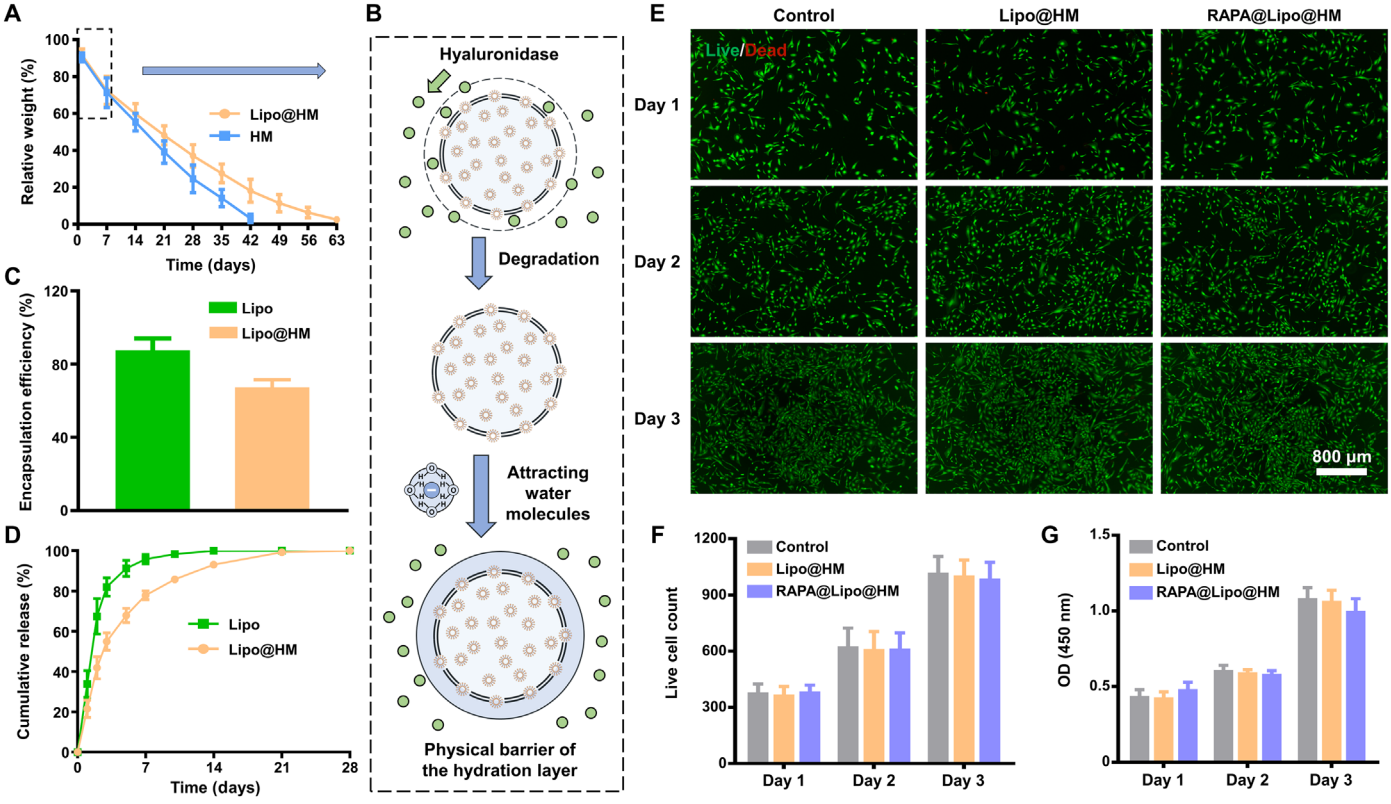

Fig. 4. Degradation, drug loading and release properties of Lipo@HMs, and biocompatibility of RAPA@Lipo@HMs. (**A**) The degradation curve of Lipo@HMs. (**B**) Schematic of the mechanism for retarding the degradation process. (**C**) The encapsulation efficiency of RAPA in liposomes and Lipo@HMs. (**D**) Release curves of RAPA releasing from liposomes and Lipo@HMs. (**E**) Live (green)/Dead (red) fluorescence results on 1, 2, and 3 days. (**F**) Viable cell count obtained from the Live/Dead staining assay. (**G**) The CCK-8 results on 1, 2, and 3 days. OD, optical density.

Live/Dead assay and cell counting kit-8 (CCK-8) assay were used to evaluate the influences of the RAPA@Lipo@HMs on the viability and proliferation of the immortalized human chondrocyte cell line (C-28/I2). As seen from Fig. 4 (E and F), nearly all cells survived a 3-day culture period without significant differences between groups. Consistent with the Live/Dead assay results, the CCK-8 assay showed that the number of cells in each group increased over time without significant differences between the groups (Fig. 4G). These results indicate that the RAPA@Lipo@HMs had favorable biocompatibility and could serve as a biolubricant to provide efficient lubrication at biological interfaces.

Effect of cellular homeostasis maintenance

Reactive oxygen species (ROS) can be produced under stress or following injury, and the accumulation of ROS can result in oxidative stress, which eventually leads to diseases such as osteoarthritis (*41*). As an evolutionarily conserved mechanism, autophagy can maintain cellular homeostasis by degrading damaged macromolecules and organelles and decreasing ROS generation, thus preventing oxidative stress–induced cellular damage (*42*–*45*).

In this study, the dichloro-dihydro-fluorescein diacetate (DCFH-DA) probe was used to detect intracellular ROS generation. As seen from Fig. 5 (A and D), the intracellular ROS level was significantly lower in the RAPA@Lipo@HM group than in the Lipo@HM and blank groups, indicating that RAPA@Lipo@HMs can increase the autophagy by delivering the autophagy activator (RAPA), which, in turn, reduces ROS generation. Increased ROS levels may trigger apoptosis (*46*). The results of the terminal deoxynucleotidyl transferase–mediated deoxyuridine triphosphate nick end labeling (TUNEL) assay showed that the number of apoptotic C-28/I2 cells was significantly less in the RAPA@Lipo@HM group than in the Lipo@HM and blank groups (Fig. 5, B and E), indicating that RAPA@Lipo@HMs can maintain cellular homeostasis and inhibit apoptosis by delivering RAPA. The Live/Dead assay and CCK-8 assay were then used to evaluate the effects of RAPA@Lipo@HMs on hydrogen peroxide (H_2O_2)–induced C-28/I2 cells. As shown in Fig. 5 (C, F, and G), the RAPA@Lipo@HM group had fewer dead cells and a higher cell proliferation rate than Lipo@HM and blank groups, indicating that RAPA@Lipo@HMs can improve cell survival and promote cell proliferation under oxidative stress.

Col2 is a major extracellular matrix component in the cartilage and serves as a marker of proliferating chondrocytes (*47*). As essential autophagic proteins, the expression of microtubule associated protein 1 light chain 3 beta (LC3B) and autophagy related 5 (ATG5) can indicate the level of autophagy activity (*48*). As the crucial enzyme in the cleavage of Col2, matrix metallopeptidase 13 (MMP13) plays a significant role in osteoarthritic cartilage matrix degradation (*49*). To determine the impact of RAPA@Lipo@HMs on the level of autophagy and the balance between cellular anabolism and catabolism, reverse transcription polymerase chain reaction (RT-PCR) was used to detect the Col2, LC3B, ATG5, and MMP13 mRNA expression levels. As shown in Fig. 6E, the RAPA@Lipo@HM group had higher Col2, LC3B, and ATG5 mRNA levels and lower MMP13 mRNA levels than the Lipo@HM and blank groups. Immunofluorescence

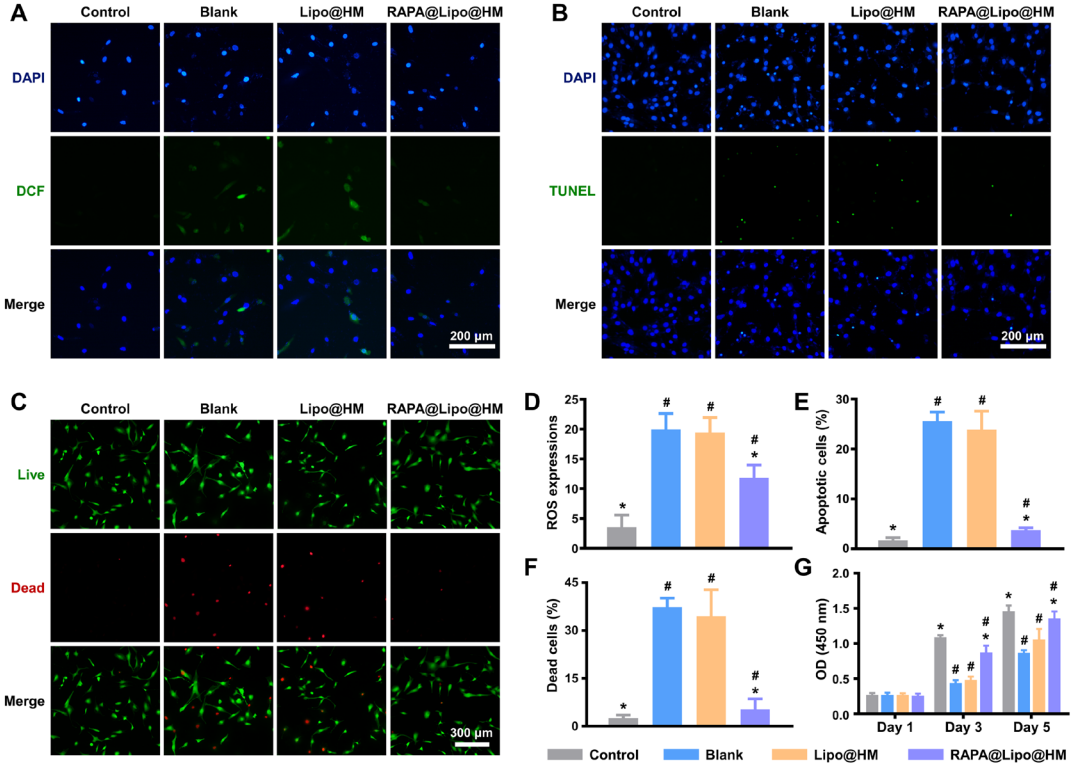

Fig. 5. RAPA@Lipo@HMs maintain cellular homeostasis. (**A**) Intracellular ROS generation measured by DCF. (**B**) Cell apoptosis measured by TUNEL staining. (**C**) Cell death measured by Live/Dead assay. (**D**) Quantitative analysis of ROS expression based on DCF fluorescence intensity. (**E**) Quantitative analysis of apoptotic cell rate based on TUNEL fluorescence intensity. (**F**) Dead cell percentage obtained from the Live/Dead staining assay. (**G**) The CCK-8 results on 1, 3, and 5 days (# and * indicate $P < 0.05$ in comparison with the control and blank groups, respectively).

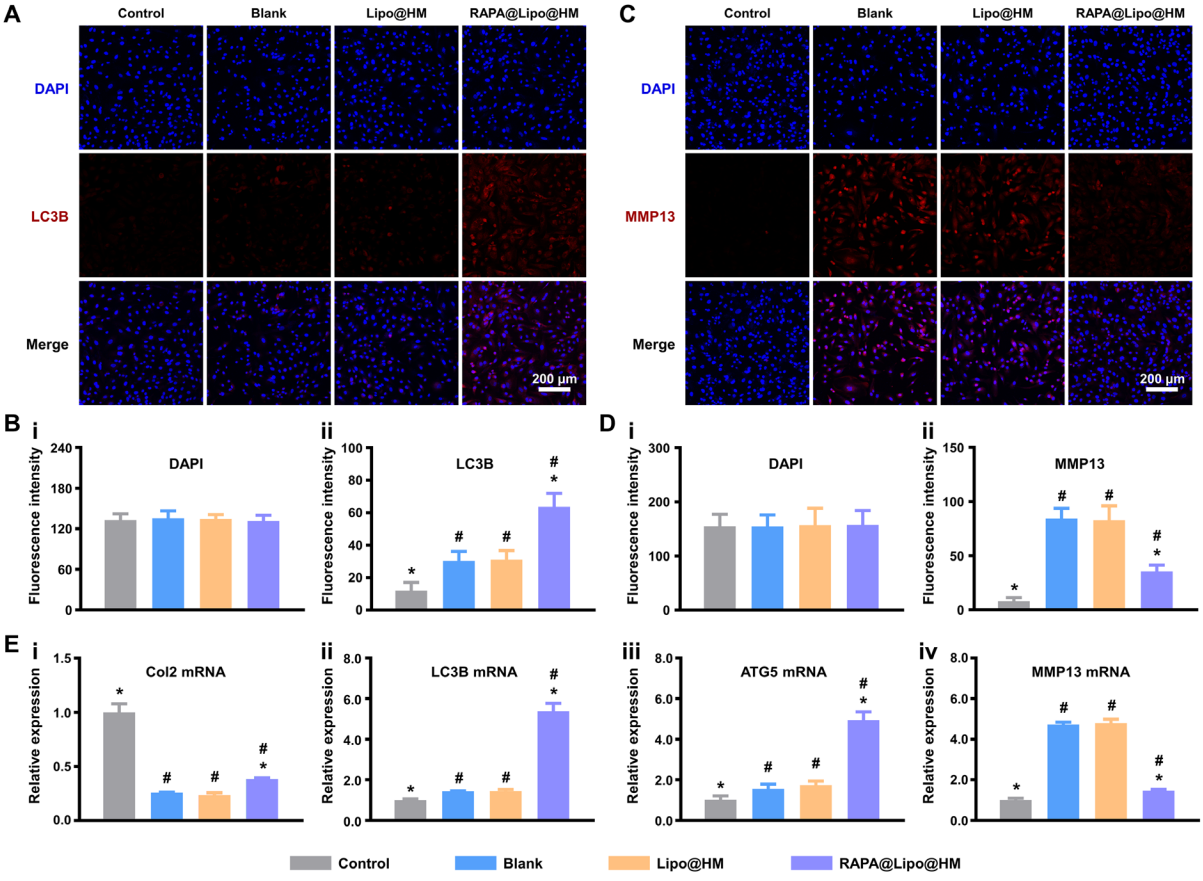

Fig. 6. RAPA@Lipo@HMs enhance autophagy, promote anabolic, and inhibit catabolic. (**A**) Representative immunofluorescence images of LC3B protein. (**B**) Quantification of (i) DAPI and (ii) LC3B fluorescences. (**C**) Representative immunofluorescence images of MMP13 protein. (**D**) Quantification of (i) DAPI and (ii) MMP13 fluorescences. (**E**) RT-PCR results showing the levels of (i) Col2, (ii) LC3B, (iii) ATG5, and (iv) MMP13 (# and * indicate $P < 0.05$ in comparison with the control and blank groups, respectively).

staining was then used to assess LC3B and MMP13. The RAPA@Lipo@HM group had a higher LC3B protein level (Fig. 6, A and B) and lower MMP13 protein level (Fig. 6, C and D) than the Lipo@HM and blank groups. These results indicate that the RAPA@Lipo@HMs promote autophagy, increase cartilage extracellular matrix secretion, and decrease MMP13 production by delivering RAPA.

In vivo retention time

For biolubrication, it is critical for the Lipo@HMs to have long retention time in the body to avoid repeated injections. In this study, we used in vivo imaging systems (IVISs) to evaluate the retention time of the fluorescently labeled Lipo@HMs and found that the fluorescence of Lipo@HMs persisted for nearly 2 months (fig. S8), indicating that Lipo@HMs can provide sustained lubrication at joint interfaces over a long period of time.

Therapeutic effect of osteoarthritis in vivo

This study used a rat osteoarthritis model induced by anterior cruciate ligament transection and medial meniscectomy to test whether the RAPA@Lipo@HMs could alleviate joint wear and reduce osteoarthritic degeneration. Osteoarthritis with progressive cartilage loss and damage usually shows joint space narrowing on an x-ray (*50*). As shown in Fig. 7 (A, C, and D), the joint space widths (JSWs) were significantly decreased in the PBS, HM, RAPA@Lipo, and Lipo@HM groups compared with the sham group. In contrast, the RAPA@Lipo@HM group significantly increased the JSW more than the PBS group; however, there was no statistical difference with the sham group, indicating that RAPA@Lipo@HMs can act as a biolubricant and as a drug delivery vehicle to ameliorate cartilage degradation. As compensation for joint damage, osteophytes are considered as another characteristic feature of osteoarthritis (*51*). As seen from Fig. 7B, osteophyte formation was observed in the PBS, HM, RAPA@Lipo, Lipo@HM, and RAPA@Lipo@HM groups, while it was absent in the sham group. Furthermore, the PBS group had ~27.7% significantly greater osteophyte volume than the RAPA@Lipo@HM group (Fig. 7E), indicating that RAPA@Lipo@HMs can alleviate joint damage, thus reducing the formation of osteophyte.

In addition to radiographic evaluation, we also used hematoxylin and eosin (HE), toluidine blue, and Safranin O-fast green staining to detect histological changes of the articular cartilage. As seen from Fig. 8 (A to C), the articular cartilage in the sham group exhibited a smooth surface, standard structural organization, normal cellularity, and a vigorous intensity of toluidine blue and Safranin O-fast green staining. However, the articular cartilage in the PBS group showed severe surface abrasion, disorganized chondrocytes, and weak toluidine blue and Safranin O-fast green staining. In comparison, no noticeable degenerative changes were observed in the RAPA@Lipo@HM group,

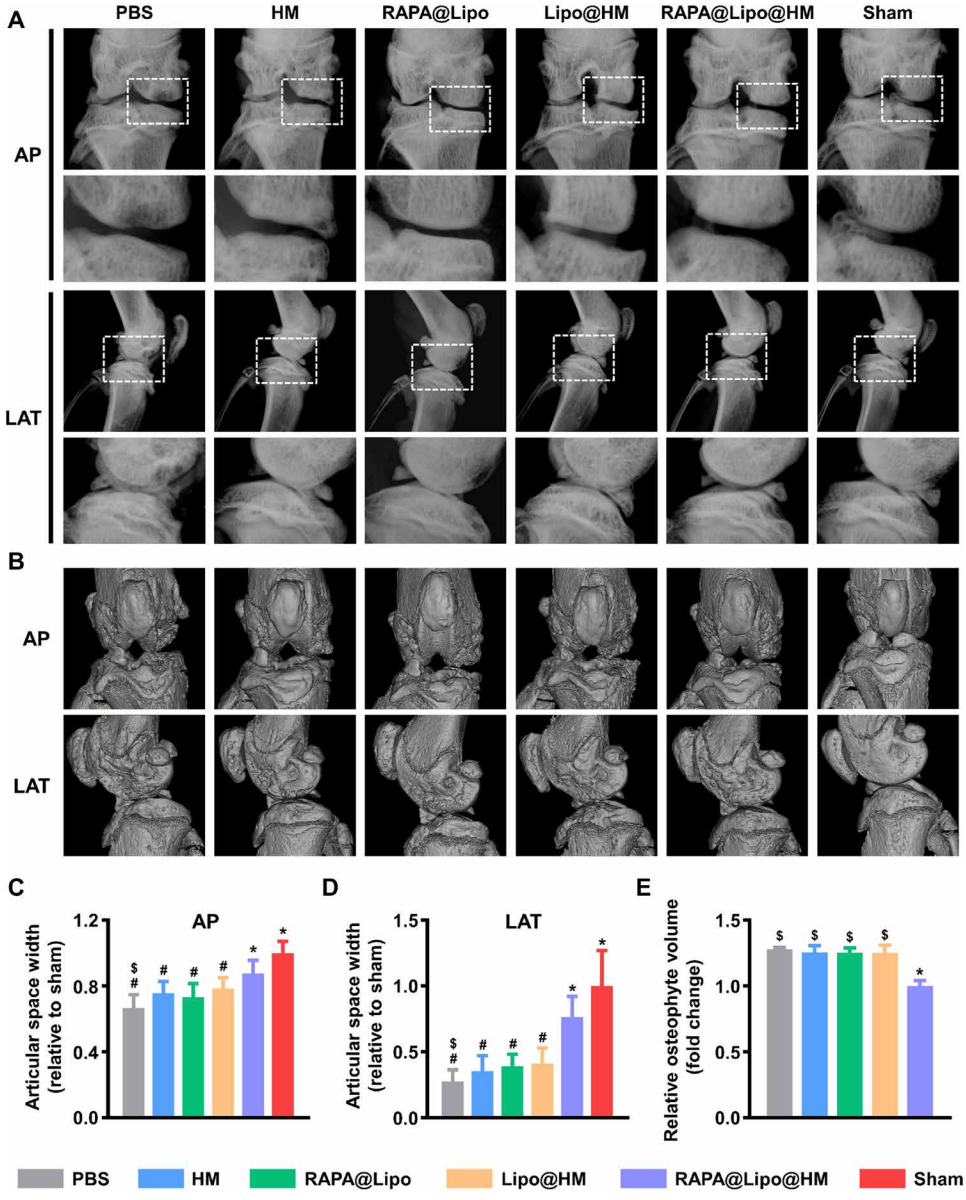

Fig. 7. RAPA@Lipo@HMs reduce joint space narrowing and osteophyte formation. (**A**) Representative x-ray images in anterior-posterior (AP) and lateral (LAT) view of the knee joint. (**B**) Representative micro-CT images in AP and LAT view of the knee joint. (**C**) The relative JSW measured from AP images. (**D**) The relative JSW measured from LAT images. (**E**) The relative osteophyte volume measured from micro-CT images (#, $, and * indicate $P < 0.05$ in comparison with the sham, RAPA@Lipo@HM, and PBS groups, respectively).

further supported by the Mankin scores (Fig. 8D). Although the articular cartilage in the Lipo@HM group showed obvious degenerative changes compared to that in the sham group, the Lipo@HM group had relative integrity and regular cartilage structure compared with the PBS group, which was supported by the Mankin scores (structure). These findings support the biolubricating effects of the Lipo@HMs.

Furthermore, the protein levels of Col2 and aggrecan were evaluated using immunohistochemistry. As shown in Fig. 9, significant decreases of Col2 and aggrecan expressions in articular cartilage were noted in the PBS, HM, RAPA@Lipo, and Lipo@HM groups when compared with the sham group; however, differences were not observed in the RAPA@Lipo@HM group. Overall, these results suggest that the RAPA@Lipo@HMs with self-renewable hydration layers can reduce friction on the articular cartilage by combining hydration lubrication and ball-bearing lubrication and release cartilage-targeting RAPA-loaded liposomes (RAPA@Lipos), which can maintain cellular homeostasis by increasing autophagy, thus alleviating joint wear and delaying the progression of osteoarthritis.

DISCUSSION

Hydration layers formed on HMs by surface coating with liposomes or polymer brushes can improve the lubrication performance of HMs. However, the lubrication deteriorates rapidly via wear once the coated layers are removed. Therefore, the HMs would have a longer service life if the hydration layers can self-renew. This study

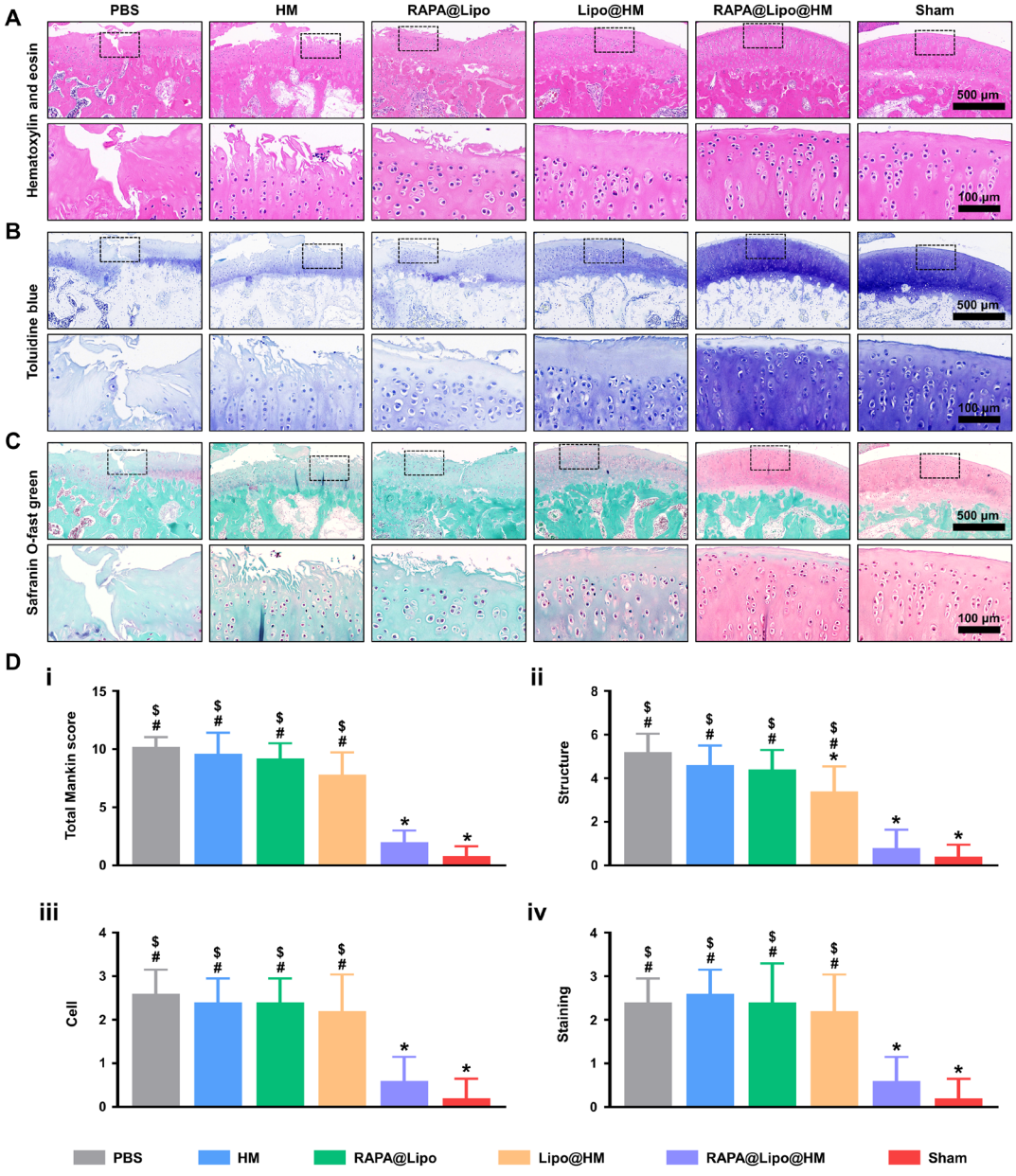

Fig. 8. Histological staining. (**A**) Representative images of HE staining, (**B**) toluidine blue staining, and (**C**) Safranin O-fast green staining from each group. (**D**) Histologic scoring of articular cartilage: (i) total Mankin scores and Mankin score presented as (ii) cartilage structure, (iii) cellular abnormalities, and (iv) matrix staining (#, $, and * indicate $P < 0.05$ in comparison with the sham, RAPA@Lipo@HM, and PBS groups, respectively).

demonstrated a simple yet effective method to create injectable microfluidic HA-based HMs with self-renewable hydration layers by incorporating liposomes. In the 3600-s friction test, with few liposomes on the outermost surfaces, the initial COF value of the newly prepared Lipo@HMs was approximately 0.04, similar to that of liposome-free HMs obtained from the following friction test. However, as the test went on, the outermost surfaces of the Lipo@HMs wore away because of friction, and more liposomes were exposed, which enabled hydration layers to form on the Lipo@HMs. In this stage, the COF value declined and stabilized at approximately 0.03 until the Lipo@HMs were squeezed out from the confined region. Notably, after a 3600-s friction test and freeze-drying and rehydration process, the COF value (0.03) of the worn Lipo@HMs was unchanged in the subsequent friction test, which is attributed to the continuous reconstruction of hydration layers through the available liposomes continuously exposed on the outer surfaces. Therefore, the Lipo@HMs with self-renewable hydration layers, which can continuously lubricate themselves as they wear, can provide efficient lubrication at biological interfaces, especially at joint interfaces where sustained friction would occur. However, osteoarthritis, the most common joint disease, is not a wear-and-tear disease, and its pathogenesis is quite complex, involving both mechanical and biological factors (*52*). Therefore, because biolubricants mainly function by reducing wear and have limited effects on cellular

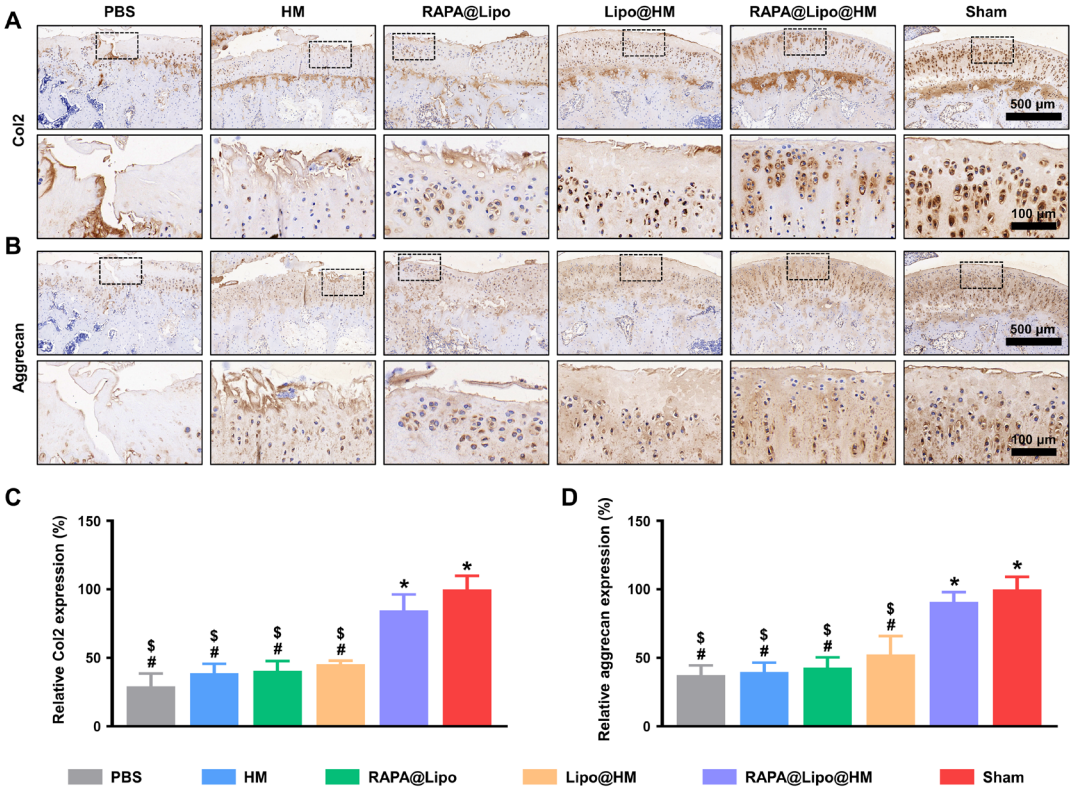

Fig. 9. Immunohistochemistry staining. (**A**) Representative images of Col2 protein immunohistochemical staining. (**B**) Representative images of aggrecan protein immunohistochemical staining. (**C**) Quantification of relative Col2 expression. (**D**) Quantification of relative aggrecan expression (#, $, and * indicate $P < 0.05$ in comparison with the sham, RAPA@Lipo@HM, and PBS groups, respectively).

homeostasis, the Lipo@HMs might not be able to prevent the development of osteoarthritis if they only serve as biolubricants. Autophagy is a homeostasis mechanism that can protect cells from stress and may be impaired under pathological conditions (e.g., osteoarthritis) (*42*). RAPA, an autophagy activator, alleviates osteoarthritis by inhibiting the mammalian target of the RAPA pathway (*36*, *44*). To avoid systemic side effects, RAPA is mainly delivered by intra-articular injection (*44*, *53*). However, because RAPA has poor water solubility, the intra-articular delivery efficiency of RAPA is quite low and requires repeated injections (*35*, *36*). Encapsulating RAPA into cationic liposomes could facilitate its solubility to achieve sustained release (*33*, *37*, *38*). In addition, the cationic liposomes can target negatively charged cartilage via electrostatic interactions, reducing off-target accumulation in other joint tissues (*31*). Nevertheless, as nanoscale substances, liposomes can be readily cleared by the reticuloendothelial system, which limits their applications (*39*). To address this issue, we incorporated the RAPA-loaded cationic liposomes within the HMs and found that RAPA@Lipo@HMs had better therapeutic results than RAPA@Lipos. Therefore, instead of acting as pure biolubricants, the constructed Lipo@HMs could also serve as drug (i.e., RAPA) delivery vehicles to maintain cellular homeostasis, providing a new strategy for treating osteoarthritis.

MATERIALS AND METHODS

HAMA synthesis

HAMA was synthesized according to a previously reported method (*54*). Briefly, 2 weight % (wt %) HA [(M_W = 74 kDa; Bloomage Freda Biopharm Co. Ltd., China) in deionized water was reacted with methacrylic anhydride (2.6-fold molar excess; Aladdin, China) at pH 8.0. The reaction solution was continuously stirred in an ice bath for 24 hours and purified by dialysis [molecular weight cut off (MWCO), 3500 Da] against deionized water for 3 days. The purified product was then lyophilized to yield a white powder. The percent methacrylation of HAMA was determined by ^{1}H NMR (600 MHz, Bruker, Germany).

Fabrication and characterization of liposomes

HSPC (EK20010) was purchased from A.V.T. Pharmaceutical Co. Ltd. (Shanghai, China), and the liposomes were prepared via a film dispersion method. Briefly, HSPC, cholesterol (Macklin, China), octadecylamine (Aladdin, China), and RAPA (Macklin, China) (40:10:4:6, w/w/w/w) were dissolved in chloroform and evaporated at 60°C for 30 min. The dried lipid film was then hydrated with deionized water and sonicated for 20 min to obtain dispersed multilamellar liposomes. The liposomes were then downsized by stepwise extrusion through 0.45- and 0.22-μm membrane filters (Millex, Ireland). The morphology of liposomes was observed under TEM (FEI Talos L120C, USA). In addition, the liposome size, PDI, and zeta potential were measured by dynamic light scattering using a Zetasizer (Malvern Nano-ZS, UK). To verify the cartilage-targeting ability of the cationic liposomes, a cartilage section was obtained from a freshly slaughtered pig knee joint and incubated with Dil (Beyotime, China)–labeled liposomes for 1 hour at 37°C. The section was then washed with PBS before observation using an LSCM (ZEISS, Germany). To confirm that the cationic liposomes can be internalized by chondrocytes, human chondrocyte C-28/I2 cells

were incubated with Dil-labeled liposomes for 12 hours and then observed under an LSCM.

Fabrication and characterization of Lipo@HMs

The pre-gel droplets were formed by emitting the 5 wt % HAMA-liposome-photoinitiator mixture (40:6:4, w/w/w) in microfluidic oil containing 95 wt % paraffin oil and 5 wt % Span 80 at the flow-focusing junction of a microfluidic device. The generated droplets were cross-linked by ultraviolet (UV) irradiation. Afterward, the cross-linked microspheres were sequentially cleaned with acetone and deionized water and then stored in deionized water before use. The morphology and size of the Lipo@HMs were observed under a bright-field microscope (LSM800, ZEISS, Germany). The surface morphology of the lyophilized Lipo@HMs was observed by SEM (FEI Sirion 200, USA). Sucrose (a cryoprotectant) was added to maintain the liposome morphology. To ensure that liposomes were successfully incorporated within the HMs, the liposomes were first labeled using DiI and then mixed with the HAMA matrix to fabricate hybrid HMs. Afterward, the Dil-labeled liposomes within the HMs were observed under an LSCM.

Tribological tests

The tribological tests were performed with reciprocating sliding using a universal materials tester (UMT-3, Bruker, Germany). All tests were conducted with an 8-mm polyethylene sphere (elastic modulus: 1 GPa; Poisson's ratio: 0.4) as the top surface and a stainless steel disk (elastic modulus: 194 GPa; Poisson's ratio: 0.3) as the bottom surface. The oscillation amplitude and frequencies were 4 mm and 1 Hz, respectively. To simulate the physiological pressure of joints (a pressure up to 25 MPa) (*55*), an average load (1 N) was applied, which created a maximum Hertz pressure of 25.68 MPa (*56*). One milliliter of the Lipo@HM suspension (1 mg/ml) was first dropped on the bottom surface, and the test was carried out for 3600 s. After the experiment, the Lipo@HMs were collected for SEM observation and the following tribological test. The lubrication performances of PBS, HMs, and the collected Lipo@HMs were evaluated and compared under the same experimental conditions. The test time was 600 s. After each test, the wear of the stainless steel disk was observed under a bright-field microscope. Next, the model SF, HMs (suspended in model SF), and collected Lipo@HMs (suspended in model SF) were subjected to 600-s friction tests under the same test conditions. The model SF was configured as described in a previous study: PBS containing HA (1.49 mg/ml), phospholipids (0.34 mg/ml), albumin (24.9 mg/ml), and γ-globulin (6.1 mg/ml) (*57*).

Degradation tests

Thirty milligrams of Lipo@HMs/HMs was immersed in 1 ml of PBS (pH 7.4) with 5 mg of hyaluronidase (Beijing Labgic Technology Co. Ltd., China) and then agitated at 37°C and 80 rpm. The supernatant was removed, and the hyaluronidase solution was replenished at 2-day intervals. At predetermined time points, the residual weight of the sample was measured and compared with its initial weight.

Drug encapsulation and release

The encapsulation efficiency of RAPA was measured using a UV-5100 UV-visible spectrophotometer (Metash, China), and the release profile of RAPA was determined according to a previous method (*39*). Briefly, RAPA@Lipos/RAPA@Lipo@HMs were packed in a dialysis bag (MWCO, 3500 Da), immersed in PBS (pH 7.4) at 37°C, and agitated at 80 rpm until the drug release was completed. At specific time points, the release medium was collected for UV analysis and replaced with an equivalent volume of PBS.

Cell biocompatibility

The immortalized human chondrocyte cell line (C-28/I2) was obtained from Otwo Biotech (China) Inc. (catalog no. HTX2308) and was used throughout this study. To examine the cytocompatibility of the RAPA@Lipo@HMs, C-28/I2 cells were seeded on the lower Transwell chambers (0.4-μm pores, Corning, USA), while the microspheres were in the upper chambers. Cells were identified by Live/Dead staining assay after coculture for 1, 2, and 3 days, and cell proliferation was assessed by a CCK-8 assay. For the Live/Dead staining assay, the cells were incubated with calcein-AM/propidium iodide (Beyotime, China) for 30 min and examined using a fluorescence microscope. For CCK-8 assay, the CCK-8 solution (Beyotime, China) was added to the culture medium, and the absorbance value (450 nm) for each well was determined 2 hours later using a FlexStation 3 microplate reader (Molecular Devices, Japan).

Osteoarthritis cell model

To simulate post-traumatic osteoarthritis, the formation of ROS increases sharply upon cartilage injury; C-28/I2 cells were seeded on the lower Transwell chambers (0.4-μm pores) and exposed to 200 μM H_2O_2 (Sigma-Aldrich, USA) (*36*). PBS, Lipo@HMs, or RAPA@Lipo@HMs were added to the upper chambers to examine the therapeutic effects of RAPA@Lipo@HMs on cellular homeostasis. C-28/I2 cells treated without H_2O_2 served as a control.

ROS detection

ROS generation was determined using a ROS Assay Kit (Beyotime, China). After incubation with or without H_2O_2 for 48 hours, the cells were stained with 10 μM DCFH-DA at 37°C for 20 min and then imaged using a fluorescence microscope.

Cell viability detection

The level of cell apoptosis was detected using a TUNEL staining kit (Beyotime, China). In brief, after a 48-hour incubation with or without H_2O_2, the cells were fixed in 4% paraformaldehyde (Servicebio, China) for 30 min and incubated with a permeabilization solution (P0097, Beyotime, China) for 5 min. The cells were then incubated with the TUNEL staining solution (Beyotime, China) for 1 hour. The cells were then stained with 4′,6-diamidino-2-phenylindole (DAPI; Beyotime, China) and observed under a fluorescence microscope. For evaluation of the live/dead cell ratio and cell proliferation, a Live/Dead staining and a CCK-8 assay were performed following the procedure described above.

Detection of mRNA expression

After incubation with or without H_2O_2 for 48 hours, the cells were subjected to RT-PCR to detect mRNA expression. Briefly, total RNA was isolated from C-28/I2 cells and reverse-transcribed using the RevertAid First Strand Complementary DNA Synthesis Kit (Thermo Fisher Scientific, USA). Afterward, RT-PCR was carried out using the ABI 7300 real-time PCR system (ABI, USA). Primer sequences of Col2, LC3B, ATG5, MMP13, and glyceraldehyde-3-phosphate dehydrogenase are shown in table S1. The relative mRNA expression was calculated using the comparative cycle threshold (CT) method (ΔΔCT method), and all the experiments were performed in triplicate.

Immunofluorescence staining

The protein levels of LC3B and MMP13 in the C-28/I2 cells were examined by immunofluorescence staining. In brief, cells were fixed with 4% paraformaldehyde for 15 min and treated with 2% bovine serum albumin for 30 min to reduce background noise. The cells were then labeled with rabbit anti-LC3B/MMP13 primary antibody (Servicebio, China) overnight at 4°C and then incubated with Cy3-conjugated goat anti-rabbit immunoglobulin G (Servicebio, China) for 50 min. The nuclei were stained with DAPI (Servicebio, China) for 10 min. The samples were viewed using an LSCM.

Evaluation of in vivo retention time

The retention time was evaluated by injecting fluorescently labeled Lipo@HMs into rat knee joints. The Lipo@HMs were labeled using Cy5.5 hydrazide (APExBIO, Shanghai, China) according to a previous method (*58*), and they were injected into the right knee. The fluorescence intensities were measured via the IVIS Spectrum System (Xenogen, USA) at different time points. The fluorescence value of the negative sample (rat knee joint injected with PBS) was used as the background fluorescence.

Rat model of osteoarthritis

Permission was granted to perform animal studies by the Research Ethics Committee of the First Affiliated Hospital of Chongqing Medical University. Male Sprague Dawley (SD) rats (12 weeks old) were randomly divided into the sham group (5 rats) and osteoarthritis group (25 rats). The rats in the osteoarthritis group were anesthetized with 3% pentobarbital sodium (40 mg/kg), and the knee joints were then subjected to anterior cruciate ligament transection and medial meniscus resection. One week after surgery, the osteoarthritis rats were further randomized into five subgroups (five rats per group), and they received 30-μl intra-articular injections of PBS, HMs, RAPA@Lipos, Lipo@HMs, or RAPA@Lipo@HMs. The injections were repeated at 4 weeks before sacrifice.

Radiographic evaluation

Eight weeks after surgery, x-ray images of the rat knee joints were obtained using a Faxitron x-ray machine (Faxitron X-ray, USA) with exposure for 10 s at 32 kV. The JSW was measured in anterior-posterior and lateral views. For further examinations, the knee joints were harvested and subjected to ex vivo microCT analyses (SkyScan 1172, Belgium).

Histologic and immunohistochemical examinations

Eight weeks after surgery, the isolated knees were paraformaldehyde-fixed, decalcified, paraffin-embedded, and then sectioned at a thickness of 5 μm. The sagittal sections were stained with HE, toluidine blue, and Safranin O-fast green for histologic analysis. The pathologic condition of the knee joints was evaluated by two blinded observers via a modified Mankin scoring system (*59*). For immunohistochemical staining, the sections were incubated with rabbit polyclonal anti-Col2/aggrecan (Servicebio, China) antibodies overnight at 4°C, followed by incubation with the secondary antibodies for 1 hour. Afterward, the paraffin sections were stained with 3,3′-diaminobenzidine (DAB) substrate. ImageJ software was used to quantify the relative expressions of Col2 and aggrecan.

Statistical analysis

Statistical analysis was implemented by SPSS 26 (SPSS Inc., USA). The differences between groups were examined with one-way analysis of variance (ANOVA) followed by Tukey's post hoc test. The level of significance was $P = 0.05$.

SUPPLEMENTARY MATERIALS

Supplementary material for this article is available at https://science.org/doi/10.1126/sciadv.abl6449

View/request a protocol for this paper from *Bio-protocol*.

REFERENCES AND NOTES

1. A. Gaisinskaya-Kipnis, J. Klein, Normal and frictional interactions between liposome-bearing biomacromolecular bilayers. *Biomacromolecules* **17**, 2591–2602 (2016).
2. B. G. Cooper, C. Bordeianu, A. Nazarian, B. D. Snyder, M. W. Grinstaff, Active agents, biomaterials, and technologies to improve biolubrication and strengthen soft tissues. *Biomaterials* **181**, 210–226 (2018).
3. Z. Chen, F. Zhang, H. Zhang, L. Cheng, K. Chen, J. Shen, J. Qi, L. Deng, C. He, H. A. Santos, W. Cui, DNA-grafted hyaluronic acid system with enhanced injectability and biostability for photo-controlled osteoarthritis gene therapy. *Adv. Sci. (Weinh)* **8**, 2004793 (2021).
4. X. Ji, Y. Yan, T. Sun, Q. Zhang, Y. Wang, M. Zhang, H. Zhang, X. Zhao, Glucosamine sulphate-loaded distearoyl phosphocholine liposomes for osteoarthritis treatment: Combination of sustained drug release and improved lubrication. *Biomater. Sci.* **7**, 2716–2728 (2019).
5. E. Andablo-Reyes, D. Yerani, M. Fu, E. Liamas, S. Connell, O. Torres, A. Sarkar, Microgels as viscosity modifiers influence lubrication performance of continuum. *Soft Matter* **15**, 9614–9624 (2019).
6. Z. Zhao, Z. Wang, G. Li, Z. Cai, J. Wu, L. Wang, L. Deng, M. Cai, W. Cui, Injectable microfluidic hydrogel microspheres for cell and drug delivery. *Adv. Funct. Mater.* **31**, 2103339 (2021).
7. A. Sarkar, F. Kanti, A. Gulotta, B. S. Murray, S. Zhang, Aqueous lubrication, structure and rheological properties of whey protein microgel particles. *Langmuir* **33**, 14699–14708 (2017).
8. J. Yang, Y. Han, J. Lin, Y. Zhu, F. Wang, L. Deng, H. Zhang, X. Xu, W. Cui, Ball-bearing-inspired polyampholyte-modified microspheres as bio-lubricants attenuate osteoarthritis. *Small* **16**, e2004519 (2020).
9. Y. Han, J. Yang, W. Zhao, H. Wang, Y. Sun, Y. Chen, J. Luo, L. Deng, X. Xu, W. Cui, H. Zhang, Biomimetic injectable hydrogel microspheres with enhanced lubrication and controllable drug release for the treatment of osteoarthritis. *Bioact. Mater.* **6**, 3596–3607 (2021).
10. S. Ma, M. Scaraggi, D. Wang, X. Wang, Y. Liang, W. Liu, D. Dini, F. Zhou, Nanoporous substrate-infiltrated hydrogels: A bioinspired regenerable surface for high load bearing and tunable friction. *Adv. Funct. Mater.* **25**, 7366–7374 (2015).
11. R. Zheng, J. Zhan, X. Wang, D. Kaplan, N. Pesika, V. T. John, Lubrication properties of phospholipid liposome coated silk microspheres. *Part. Part. Syst. Charact.* **30**, 133–137 (2013).
12. S. Oak, L. Pashazanusi, S. B. Sengel, M. Omarova, J. L. Hemstock, W. He, J. He, V. John, N. Sahiner, N. S. Pesika, Tunable friction through stimuli responsive hybrid carbon microspheres. *Langmuir* **35**, 15849–15854 (2019).
13. J. Li, W. Cao, Z. Wang, M. Ma, J. Luo, Origin of hydration lubrication of zwitterions on graphene. *Nanoscale* **10**, 16887–16894 (2018).
14. U. Raviv, S. Giasson, N. Kampf, J. F. Gohy, R. Jérôme, J. Klein, Lubrication by charged polymers. *Nature* **425**, 163–165 (2003).
15. L. Ma, A. Gaisinskaya-Kipnis, N. Kampf, J. Klein, Origins of hydration lubrication. *Nat. Commun.* **6**, 6060 (2015).
16. G. Liu, Z. Liu, N. Li, X. Wang, F. Zhou, W. Liu, Hairy polyelectrolyte brushes-grafted thermosensitive microgels as artificial synovial fluid for simultaneous biomimetic lubrication and arthritis treatment. *ACS Appl. Mater. Interfaces* **6**, 20452–20463 (2014).
17. J. Zhang, S. Xiao, M.-x. Shen, L. Sun, F. Chen, P. Fan, M. Zhong, J. Yang, Aqueous lubrication of poly(*N*-hydroxyethyl acrylamide) brushes: A strategy for their enhanced load bearing capacity and wear resistance. *RSC Adv.* **6**, 21961–21968 (2016).
18. M.-X. Shen, Z.-X. Zhang, J.-T. Yang, G.-Y. Xiong, Wetting behavior and tribological properties of polymer brushes on laser-textured surface. *Polymers (Basel)* **11**, 981 (2019).
19. Y. Duan, Y. Liu, J. Li, S. Feng, S. Wen, AFM study on superlubricity between Ti6Al4V/polymer surfaces achieved with liposomes. *Biomacromolecules* **20**, 1522–1529 (2019).
20. M. Rong, H. Liu, M. Scaraggi, Y. Bai, L. Bao, S. Ma, Z. Ma, M. Cai, D. Dini, F. Zhou, High lubricity meets load capacity: Cartilage mimicking bilayer structure by brushing up stiff hydrogels from subsurface. *Adv. Funct. Mater.* **30**, 2004062 (2020).
21. M. Yu, M. Liu, L. Zhang, M. Li, Y. Hou, D. Wang, S. Fu, Liquid-repellent and self-repairing lubricant-grafted surfaces constructed by thiol-ene click chemistry using activated hollow silica as the lubricant reservoir. *J. Colloid Interface Sci.* **586**, 279–291 (2021).
22. J. Seror, L. Zhu, R. Goldberg, A. J. Day, J. Klein, Supramolecular synergy in the boundary lubrication of synovial joints. *Nat. Commun.* **6**, 6497 (2015).

23. R. Sorkin, N. Kampf, L. Zhu, J. Klein, Hydration lubrication and shear-induced self-healing of lipid bilayer boundary lubricants in phosphatidylcholine dispersions. *Soft Matter* **12**, 2773–2784 (2016).
24. Z. Liu, W. Lin, Y. Fan, N. Kampf, Y. Wang, J. Klein, Effects of hyaluronan molecular weight on the lubrication of cartilage-emulating boundary layers. *Biomacromolecules* **21**, 4345–4354 (2020).
25. W. Lin, M. Kluzek, N. Iuster, E. Shimoni, N. Kampf, R. Goldberg, J. Klein, Cartilage-inspired, lipid-based boundary-lubricated hydrogels. *Science* **370**, 335–338 (2020).
26. L. Zhu, J. Seror, A. J. Day, N. Kampf, J. Klein, Ultra-low friction between boundary layers of hyaluronan-phosphatidylcholine complexes. *Acta Biomater.* **59**, 283–292 (2017).
27. X. Zhang, S. Koo, J. H. Kim, X. Huang, N. Kong, L. Zhang, J. Zhou, J. Xue, M. B. Harris, W. Tao, J. S. Kim, Nanoscale materials-based platforms for the treatment of bone-related diseases. *Matter* **4**, 2727–2764 (2021).
28. Y. Wang, W. Zhang, P. Sun, Y. Cai, W. Xu, Q. Fan, Q. Hu, W. Han, A novel multimodal NIR-II nanoprobe for the detection of metastatic lymph nodes and targeting chemo-photothermal therapy in oral squamous cell carcinoma. *Theranostics* **9**, 391–404 (2019).
29. A. Raj, M. Wang, T. Zander, D. C. F. Wieland, X. Liu, J. An, V. M. Garamus, R. Willumeit-Römer, M. Fielden, P. M. Claesson, A. Dėdinaitė, Lubrication synergy: Mixture of hyaluronan and dipalmitoylphosphatidylcholine (DPPC) vesicles. *J. Colloid Interface Sci.* **488**, 225–233 (2017).
30. A. G. Bajpayee, A. J. Grodzinsky, Cartilage-targeting drug delivery: Can electrostatic interactions help? *Nat. Rev. Rheumatol.* **13**, 183–193 (2017).
31. S. B. Brown, L. Wang, R. R. Jungels, B. Sharma, Effects of cartilage-targeting moieties on nanoparticle biodistribution in healthy and osteoarthritic joints. *Acta Biomater.* **101**, 469–483 (2020).
32. C. M. Hartford, M. J. Ratain, Rapamycin: Something old, something new, sometimes borrowed and now renewed. *Clin. Pharmacol. Ther.* **82**, 381–388 (2007).
33. K. K. Ewert, P. Scodeller, L. Simón-Gracia, V. M. Steffes, E. A. Wonder, T. Teesalu, C. R. Safinya, Cationic liposomes as vectors for nucleic acid and hydrophobic drug therapeutics. *Pharmaceutics* **13**, 1365 (2021).
34. G. Catavitello, Y. Ivanenko, F. Lacquaniti, A kinematic synergy for terrestrial locomotion shared by mammals and birds. *eLife* **7**, e38190 (2018).
35. M. B. Abud, R. N. Louzada, D. L. C. Isaac, L. G. Souza, R. G. Dos Reis, E. M. Lima, M. P. de Ávila, In vivo and in vitro toxicity evaluation of liposome-encapsulated sirolimus. *Int. J. Retina Vitreous* **5**, 35 (2019).
36. K. M. Dhanabalan, V. K. Gupta, R. Agarwal, Rapamycin-PLGA microparticles prevent senescence, sustain cartilage matrix production under stress and exhibit prolonged retention in mouse joints. *Biomater. Sci.* **8**, 4308–4321 (2020).
37. C. H. Chen, S. M. Kuo, Y. C. Tien, P. C. Shen, Y. W. Kuo, H. H. Huang, Steady augmentation of anti-osteoarthritic actions of rapamycin by liposome-encapsulation in collaboration with low-intensity pulsed ultrasound. *Int. J. Nanomedicine* **15**, 3771–3790 (2020).
38. J. Yang, X. Zhang, C. Liu, Z. Wang, L. Deng, C. Feng, W. Tao, X. Xu, W. Cui, Biologically modified nanoparticles as theranostic bionanomaterials. *Prog. Mater. Sci.* **118**, 100768 (2021).
39. J. Yang, Y. Zhu, F. Wang, L. Deng, X. Xu, W. Cui, Microfluidic liposomes-anchored microgels as extended delivery platform for treatment of osteoarthritis. *Chem. Eng. J.* **400**, 126004 (2020).
40. X. Zhang, L. Li, J. Ouyang, L. Zhang, J. Xue, H. Zhang, W. Tao, Electroactive electrospun nanofibers for tissue engineering. *Nano Today* **39**, 101196 (2021).
41. R. Liang, J. Zhao, B. Li, P. Cai, X. J. Loh, C. Xu, P. Chen, D. Kai, L. Zheng, Implantable and degradable antioxidant poly(ε-caprolactone)-lignin nanofiber membrane for effective osteoarthritis treatment. *Biomaterials* **230**, 119601 (2020).
42. J. S. Rockel, M. Kapoor, Autophagy: Controlling cell fate in rheumatic diseases. *Nat. Rev. Rheumatol.* **12**, 517–531 (2016).
43. N. Mizushima, B. Levine, A. M. Cuervo, D. J. Klionsky, Autophagy fights disease through cellular self-digestion. *Nature* **451**, 1069–1075 (2008).
44. T. Matsuzaki, T. Matsushita, Y. Tabata, T. Saito, T. Matsumoto, K. Nagai, R. Kuroda, M. Kurosaka, Intra-articular administration of gelatin hydrogels incorporating rapamycin-micelles reduces the development of experimental osteoarthritis in a murine model. *Biomaterials* **35**, 9904–9911 (2014).
45. W. Liu, L. Xu, X. Wang, D. Zhang, G. Sun, M. Wang, M. Wang, Y. Han, R. Chai, H. Wang, PRDX1 activates autophagy via the PTEN-AKT signaling pathway to protect against cisplatin-induced spiral ganglion neuron damage. *Autophagy* **2021**, 1–23 (2021).
46. T. Juhász, C. Matta, É. Katona, C. Somogyi, R. Takács, P. Gergely, L. Csernoch, G. Panyi, G. Tóth, D. Reglődi, A. Tamás, R. Zákány, Pituitary adenylate cyclase activating polypeptide (PACAP) signalling exerts chondrogenesis promoting and protecting effects: Implication of calcineurin as a downstream target. *PLOS ONE* **9**, e91541 (2014).
47. L. Xing, D. Chen, B. F. Boyce, Mice deficient in NF-κB p50 and p52 or RANK have defective growth plate formation and post-natal dwarfism. *Bone Res.* **1**, 336–345 (2013).
48. J. K. Meckes, B. Caramés, M. Olmer, W. B. Kiosses, S. P. Grogan, M. K. Lotz, D. D. D'Lima, Compromised autophagy precedes meniscus degeneration and cartilage damage in mice. *Osteoarthr. Cartil.* **25**, 1880–1889 (2017).
49. Q. Hu, M. Ecker, Overview of MMP-13 as a promising target for the treatment of osteoarthritis. *Int. J. Mol. Sci.* **22**, 1742 (2021).
50. T. Paixao, M. D. DiFranco, R. Ljuhar, D. Ljuhar, C. Goetz, Z. Bertalan, H. P. Dimai, S. Nehrer, A novel quantitative metric for joint space width: Data from the Osteoarthritis Initiative (OAI). *Osteoarthr. Cartil.* **28**, 1055–1061 (2020).
51. L. Lieben, Osteoarthritis: Osteophyte formation involves PAR2. *Nat. Rev. Rheumatol.* **12**, 70–71 (2016).
52. D. J. Hunter, S. Bierma-Zeinstra, Osteoarthritis. *Lancet* **393**, 1745–1759 (2019).
53. J. Bao, Z. Chen, L. Xu, L. Wu, Y. Xiong, Rapamycin protects chondrocytes against IL-18-induced apoptosis and ameliorates rat osteoarthritis. *Aging (Albany NY)* **12**, 5152–5167 (2020).
54. B. S. Spearman, N. K. Agrawal, A. Rubiano, C. S. Simmons, S. Mobini, C. E. Schmidt, Tunable methacrylated hyaluronic acid-based hydrogels as scaffolds for soft tissue engineering applications. *J. Biomed. Mater. Res. A* **108**, 279–291 (2020).
55. A. Dėdinaitė, D. C. F. Wieland, P. Bełdowski, P. M. Claesson, Biolubrication synergy: Hyaluronan-phospholipid interactions at interfaces. *Adv. Colloid Interface Sci.* **274**, 102050 (2019).
56. H. Chen, T. Sun, Y. Yan, X. Ji, Y. Sun, X. Zhao, J. Qi, W. Cui, L. Deng, H. Zhang, Cartilage matrix-inspired biomimetic superlubricated nanospheres for treatment of osteoarthritis. *Biomaterials* **242**, 119931 (2020).
57. D. Nečas, K. Sadecká, M. Vrbka, A. Galandáková, M. A. Wimmer, J. Gallo, M. Hartl, The effect of albumin and γ-globulin on synovial fluid lubrication: Implication for knee joint replacements. *J. Mech. Behav. Biomed. Mater.* **113**, 104117 (2021).
58. M. Xavier, L. García-Hevia, I. R. Amado, L. Pastrana, C. Gonçalves, In vitro intestinal uptake and permeability of fluorescently-labelled hyaluronic acid nanogels. *Int. J. Nanomedicine* **14**, 9077–9088 (2019).
59. S. J. Moon, Y. J. Woo, J. H. Jeong, M. K. Park, H. J. Oh, J. S. Park, E. K. Kim, M. L. Cho, S. H. Park, H. Y. Kim, J. K. Min, Rebamipide attenuates pain severity and cartilage degeneration in a rat model of osteoarthritis by downregulating oxidative damage and catabolic activity in chondrocytes. *Osteoarthr. Cartil.* **20**, 1426–1438 (2012).

Acknowledgments

Funding: This work was supported by the National Key Research and Development Program of China (2020YFA0908200), the National Natural Science Foundation of China (81930051 and 81972069), Shanghai Jiao Tong University "Medical and Research" Program (ZH2018ZDA04), and Shanghai Municipal Education Commission—Gaofeng Clinical Medicine Grant Support (20171906). **Author contributions:** Y.L. and Y.W. performed experiments, analyzed the data, and wrote an initial draft of the manuscript. J.S., Z.C., C.Z., and H.C. analyzed the data. X.L. supervised the research. N.H. derived the theory and supervised the research. W.C. and W.H. derived the theory, supervised the research, discussed and interpreted results, and edited the manuscript. **Competing interests:** The authors declare that they have no competing interests. **Data and materials availability:** All data needed to evaluate the conclusions in the paper are present in the paper and/or the Supplementary Materials.

Submitted 27 July 2021
Accepted 9 December 2021
Published 2 February 2022
10.1126/sciadv.abl6449